

We are IntechOpen, the world's leading publisher of Open Access books Built by scientists, for scientists

6,900

Open access books available

186,000

International authors and editors

200M

Downloads

Our authors are among the

154

Countries delivered to

TOP 1%

most cited scientists

12.2%

Contributors from top 500 universities



WEB OF SCIENCE™

Selection of our books indexed in the Book Citation Index
in Web of Science™ Core Collection (BKCI)

Interested in publishing with us?
Contact book.department@intechopen.com

Numbers displayed above are based on latest data collected.
For more information visit www.intechopen.com



Interaction of Longitudinal Vortices and the Effect on Fluid Flow and Heat Transfer

Kewei Song

Additional information is available at the end of the chapter

<http://dx.doi.org/10.5772/60007>

1. Introduction

Developing and innovating new techniques to enhance the heat transfer of a new compact heat exchanger is not only useful but also necessary for energy saving. The flow with longitudinal velocity components is an important phenomenon in fluid dynamics and heat transfer. Longitudinal vortices are generated by flow separation along the side edges of the vortex generators (VGs) due to the pressure differences between the upstream and the downstream sides and are perpendicular to the main flow direction. A description of the typical vortices structure formed by a delta winglet VG is given in some publications [1, 2]. There is a main vortex that is formed as a result of the flow separating in the tip of the half-delta wing and rolling up due to the lower pressure in the back side of the VG. Then there is a corner vortex that is horseshoe-like vortex formed in the corner between the front side of the VG and the fin. Finally, there is an induced secondary vortex formed in the corner between the back side of the wing and the fin as a result of the redirection of the near wall flow caused by the lower pressure behind the generator.

The longitudinal vortices can potentially enhance heat transfer with small pressure loss penalty and a better heat transfer effect than that of latitudinal vortices. The longitudinal vortices can cause bulk fluid mixing, boundary-layer modification, flow destabilization, and thereby enhance convective heat transfer. Setting protrusions that can generate longitudinal vortices on the fin surface is a promising technique to enhance the airside heat transfer. There are many protrusions that can generate longitudinal vortices. Vortex generators (VGs) are among the most popular actuators for the fin-side heat transfer enhancement. The winglet VG is capable of enhancing heat transfer with less increase in pressure penalty compared to other type of protrusions. A thorough review of the progress made in the application of longitudinal VGs is performed in reference [3].

In order to obtain a better heat transfer performance, researchers always try to punch lots of VGs out of the fin surface. However, the increasing number of VGs is not necessarily linked with the rise in heat transfer performance augmentation. This is because the vortices not only change the boundary layer structure but also interact with each other when they meet in the flow channel and the interaction of vortices affects the intensity of vortices and their effect on heat transfer enhancement. Experimental and numerical studies focusing on the interactions between vortices and boundary layers have been carried out in references [4–6]. The experimental investigation about the interaction vortices and the boundary layers indicated that in the region where two neighboring vortices induced flow toward the heat transfer surface, local heat transfer was locally enhanced. Conversely, in the regions where neighboring vortices induced outflow departs the heat transfer surface, the local heat transfer was decreased. Close proximity of other vortices strongly affects the spreading of the vorticity. The heat transfer modification produced by the vortex was strongly dependent on vortex interaction. These previous works have shown that the strength of the vortices interaction with the wall is strongly dependent on the arrangement of vortices in the array. However, seldom works consider the interaction of longitudinal vortices and their effect on heat transfer. The effect of interaction of longitudinal vortices generated by winglet VGs on heat transfer enhancement of a flat tube bank fin heat exchanger was qualitatively analyzed in reference [7]. The quantitative study of the interaction of longitudinal vortices was seldom reported due to the lack of parameter that can define the intensity of longitudinal vortices. A nondimensional parameter Se was defined for the intensity of secondary flow in reference [8]. The parameter Se provides a powerful tool for the quantitative study of the interaction between longitudinal vortices. By using Se , quantitative studies about the interaction of longitudinal vortices generated by VGs mounted on the fin surfaces of flat tube bank fin heat exchanger were carried out in references [9, 10].

In this chapter, the nondimensional parameter Se that can be used for the description of the intensity of the longitudinal vortices is introduced first, then the interaction of counterrotating longitudinal vortices generated by VGs is quantitatively studied, and the effect of interaction on the intensity of vortices and heat transfer are discussed in detail by using the nondimensional parameter Se .

2. Physical model

As stated above, the longitudinal vortices can provide good performance for fluid flow and heat transfer enhancement. As the intensity of the longitudinal vortices decreases along the main flow direction, in order to obtain a high intensity of longitudinal vortices in the flow field, lots of VGs are always protruded into the flow field. Different arrangements of VGs will generate longitudinal vortices with different intensity and different rotating directions. These vortices with different rotating directions will inevitably meet and interact with each other when they are flowing downward. The interaction between these vortices affects not only the intensity of the vortices but also the heat transfer enhancement of the longitudinal vortices.

For the plate-fin heat exchangers, there are many rows of VGs, and interaction between these vortices generated by different VGs will be a common physics phenomenon. This chapter focuses on the interaction between two counterrotating longitudinal vortices with different transversal pitches.

The physical model is shown in Figure 1. The flow channel is formed by two plain fins. Two winglet VGs with a certain longitudinal pitch are mounted on the bottom fin surface. The VGs are mounted around the longitudinal center line of the channel and the longitudinal pitch b is fixed to $3.5H$, where $H = 2 \text{ mm}$ is the height of the flow channel. The height of the VGs is $h = 0.7H$, and the length of the base is $l = 2h$. The attack angle of VG is $\theta = 35^\circ$. The first VG is placed $5H$ away from the inlet. The width and the length of the channel are $S = 7H$ and $L = 22H$, respectively. The transversal pitches of the VGs and the ratio of transversal pitch to the projected length of the base of VGs are summarized in Table 1. When the value of c changes from c_1 to c_8 , there are two different arrangement relationships between the VGs. The schematic view and the front view of the two different arrangements of the VGs are shown in Figure 1(b) and (c), respectively. For convenience, the front VG is named as VG1 and the latter is named as VG2. Figure 2 shows the longitudinal vortices in the cross section for different arrangements of VGs.

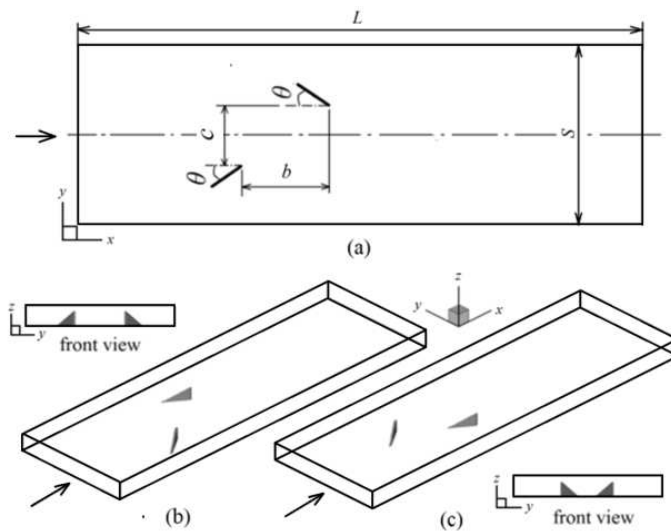


Figure 1. Schematic view of the physical model.

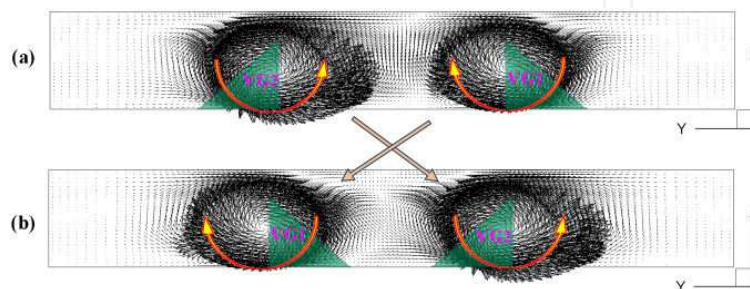


Figure 2. Relationship between the arrangement of VGs and the longitudinal vortices.

Pitch no.	c1	c2	c3	c4	c5	c6	c7	c8
<i>c</i> (mm)	4.818	3.212	1.606	0.0	1.606	3.212	4.818	6.424
<i>c</i> /(<i>l</i> sinθ)	3	2	1	0	1	2	3	4

Table 1. Transversal pitches of VGs

3. Governing equations and boundary condition

In the case of the heat exchangers, the fin spacing is small and the flow in gas side is usually laminar. With this application in mind, the delta winglet VG in a laminar developing flow is considered in the present investigation. In such case, the compact forms of governing equations in physical space are as follows:

Continuity equation

$$\frac{\partial}{\partial x_i}(\rho u_i) = 0 \quad (1)$$

Momentum equations

$$\frac{\partial}{\partial x_i}(\rho u_i u_k) = \frac{\partial}{\partial x_i} \left(\mu \frac{\partial u_k}{\partial x_i} \right) - \frac{\partial p}{\partial x_k} \quad (k = 1, 2, 3) \quad (2)$$

Energy equation

$$\frac{\partial}{\partial x_i}(\rho c_p u_i T) = \frac{\partial}{\partial x_i} \left(\lambda \frac{\partial T}{\partial x_i} \right) \quad (3)$$

For developing flow, the boundary conditions at the inlet surface are given as follows:

$$u(x, y, z)|_{\text{inlet}} = u_{\text{in}}, v(x, y, z)|_{\text{inlet}} = 0, w(x, y, z)|_{\text{inlet}} = 0, T(x, y, z)|_{\text{inlet}} = T_{\text{in}} \quad (4)$$

At the outlet surface

$$\frac{\partial}{\partial x} u(x, y, z) = 0, \frac{\partial}{\partial x} v(x, y, z) = 0, \frac{\partial}{\partial x} w(x, y, z) = 0, \frac{\partial}{\partial x} T(x, y, z) = 0 \quad (5)$$

At the symmetric surfaces

$$v(x, y, z) = 0, \frac{\partial}{\partial y} u(x, y, z) = 0, \frac{\partial}{\partial y} w(x, y, z) = 0, \frac{\partial}{\partial y} T(x, y, z) = 0 \quad (6)$$

At the solid surfaces, constant temperature and no-slip condition for velocity are applied as follows:

$$u(x, y, z) = 0, v(x, y, z) = 0, w(x, y, z) = 0, T = T_w \quad (7)$$

The Reynolds number is

$$Re = \rho \cdot u_m \cdot d_h / \mu \quad (8)$$

The local Nusselt number is determined by

$$Nu_{local} = -d_h \frac{\partial T}{\partial n} / (T_w - T_{bulk}) \quad (9)$$

T_{bulk} is the cross-sectional averaged temperature:

$$T_{bulk} = \frac{\int_A T dA}{A} \quad (10)$$

The span-averaged Nu_s is obtained by averaging Nu_{local} over the span strip fin surfaces at position x :

$$Nu_s(x) = \int_0^s Nu_{local}(x, y) dy / \left(\int_0^s dy \right) \quad (11)$$

The overall average Nu is obtained by averaging Nu_{local} over the entire fin surfaces:

$$Nu = \frac{\iint_A Nu_{local} dA}{\iint_A dA} \quad (12)$$

4. Parameter for the intensity of longitudinal vortices

If the main flow direction is along the x -axis, the secondary flow is the flow in the cross section normal to x -axis. Thus, secondary flow relates to the velocity components' gradients in the cross section: $\partial w / \partial y - \partial v / \partial z$. The vorticity component along the main flow direction represents the angle velocity of flow that rotates around the axis having the direction along the main flow.

According to reference [8], the product of the absolute vorticity flux and the hydraulic diameter is the characteristic velocity of secondary flow, as follows:

$$U_s = d_h J_{ABS}^n \quad (13)$$

U_s is the characteristic velocity of secondary flow, d_h is the hydraulic diameter, and J_{ABS}^n is the absolute vorticity flux in normal direction of the cross section. In references [11, 12], J_{ABS}^n is written as follows:

$$J_{ABS}^n = \frac{1}{A(x)} \iint_{A(x)} |\omega^n| dA \quad (14)$$

where A is the cross-sectional area, and ω^n is the component of ω normal to the cross section.

Based on the study of J_{ABS}^n , a nondimensional parameter Se is defined for the intensity of secondary flow in reference [8]. Se is defined as follows:

$$Se = \frac{\rho d_h U_s}{\mu} \quad (15)$$

Se has the same form as the definition of Re , but the physical meaning is quite different. Se represents the ratio of inertial force to viscous force, which are induced by the secondary flow. Re represents the ratio of inertial force to viscous force, which are induced by the main flow. The cross-sectional average value of Se at position x is a local average intensity of secondary flow in a small volume:

$$Se_s(x) = \frac{\rho d_h^2}{\mu} \iint_{A(x)} |\omega^n| dA / \iint_{A(x)} dA \quad (16)$$

The volume-averaged value of Se is obtained by integrating the local value of Se over the total flow field:

$$Se = \frac{\rho d_h^2}{\mu} \iiint_V |\omega^n| dV / \iiint_V dV \quad (17)$$

5. Numerical method

The simulation domain in physical space (x, y, z) coordinates is transformed into a rectangular parallelepiped in the computational space (ξ, η, ζ) coordinates. The governing equations and

boundary conditions are transformed into the computational space and discretized by the control volume method in a collocated grid system. The power scheme is used to discretize the convective terms, while the central difference scheme is employed to discretize the diffusion terms. The SIMPLE algorithm is used to obtain the numerical solution of continuity and momentum equations.

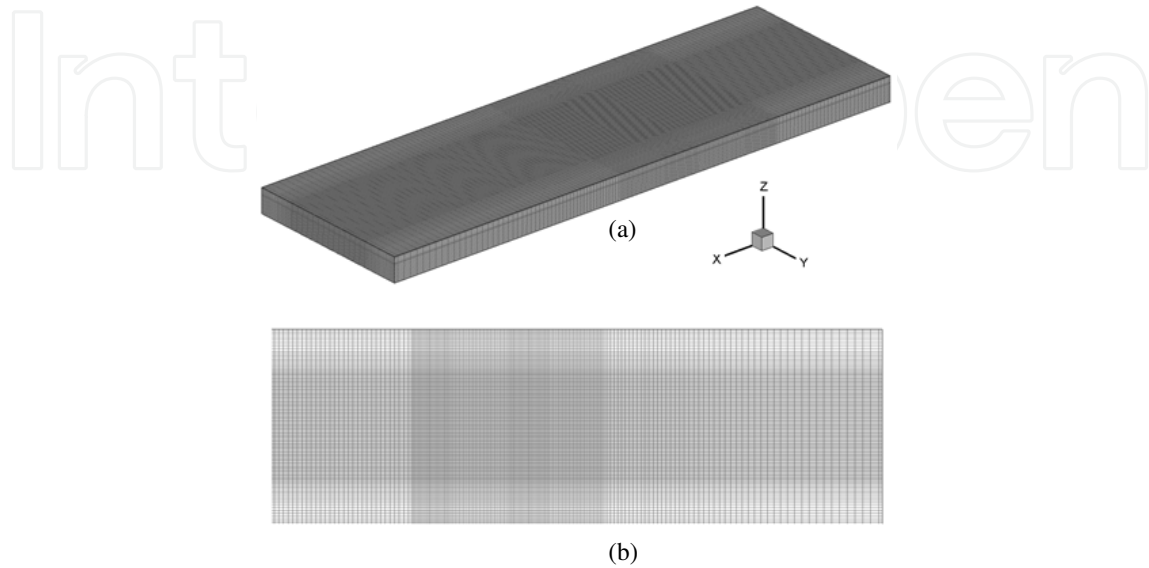


Figure 3. Grid system used for the simulation domain, (a) schematic view of the three-dimensional grid, (b) grid in the x - y plane.

A typical structured grid system used in the present study is shown in Figure 3. Figure 3(a) shows the schematic view of the three-dimensional grid system, and Figure 3(b) is the grid in x - y plane. In the region where VGs are mounted, in order to keep the shape of the VG, fine and uniform grids are needed in each direction and the grid in each direction must keep a proportional interval in the region. In the numerical investigations about the application of VGs, most of the VGs are idealized as of zero thickness. In the present study, the VGs with finite thickness are considered to render the computations more realistic. Grid-independent performance is carried out at three different grid systems with the numbers of the fine grid twice the coarse grid in each coordinate direction, as shown in Table 2. The differences of the grid independent of Nu and f are less than 1% for the studied three grid systems. Considering the mesh quality and the occupation of computer resources, all the results are obtained using the grid size of $194 \times 142 \times 32$.

Grid ($x \times y \times z$)	Nu	f
$134 \times 98 \times 22$	6.6418	0.0580
$194 \times 142 \times 32$	6.6073	0.0578
$258 \times 190 \times 44$	6.6291	0.0582

Table 2. Grid independence

6. Results and discussion

The generation of longitudinal vortices and the subsequent disruption of thermal boundary layers are the prime movers of heat transfer augmentation. Thus, the flow field attracts special attention. In order to show the development of the flow field, eight cross sections are selected as shown in Figure 4, the locations of these selected sections are summarized in Table 3.

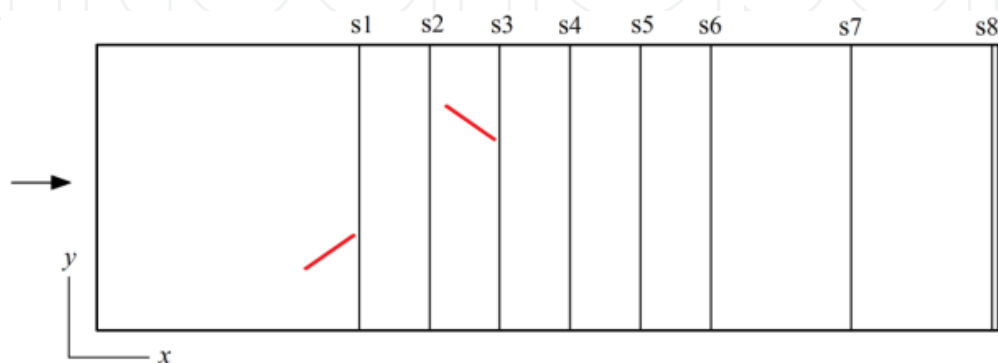


Figure 4. The selected cross-sections.

Cross section	s1	s2	s3	s4	s5	s6	s7	s8
x/L	0.291	0.368	0.448	0.525	0.602	0.682	0.836	0.993

Table 3. Cross-sectional positions

6.1. Effect of interaction of longitudinal vortices on the flow field

The velocity vectors on the cross sections for transversal pitch $c2$ and $c6$ with $Re = 1800$ are shown in Figures 5 and 6, respectively. When fluid passes through the VGs, strong longitudinal vortices with counterrotating directions are generated. The vortices that have clockwise rotating directions on cross sections $s1$ to $s8$ are generated by the first VG, and the vortices that have anticlockwise rotating directions on cross sections $s3$ to $s8$ are generated by the second VG. Comparing the vortices on different cross sections, the intensity of the longitudinal vortices decreases gradually downward.

Figures 5 and 6 correspond to the arrangements of Figure 1(b) and (c), respectively. By comparing the flow field structure in Figures 5 and 6, one can find that the flow field structures in the common region between the vortices are different. In Figure 5, the fluid in the common region is directed away from the bottom fin surface and forms a common flow-up flow field structure. However, in Figure 6, the fluid in the common region is directed toward the bottom fin surface and forms a common flow-down flow field structure.

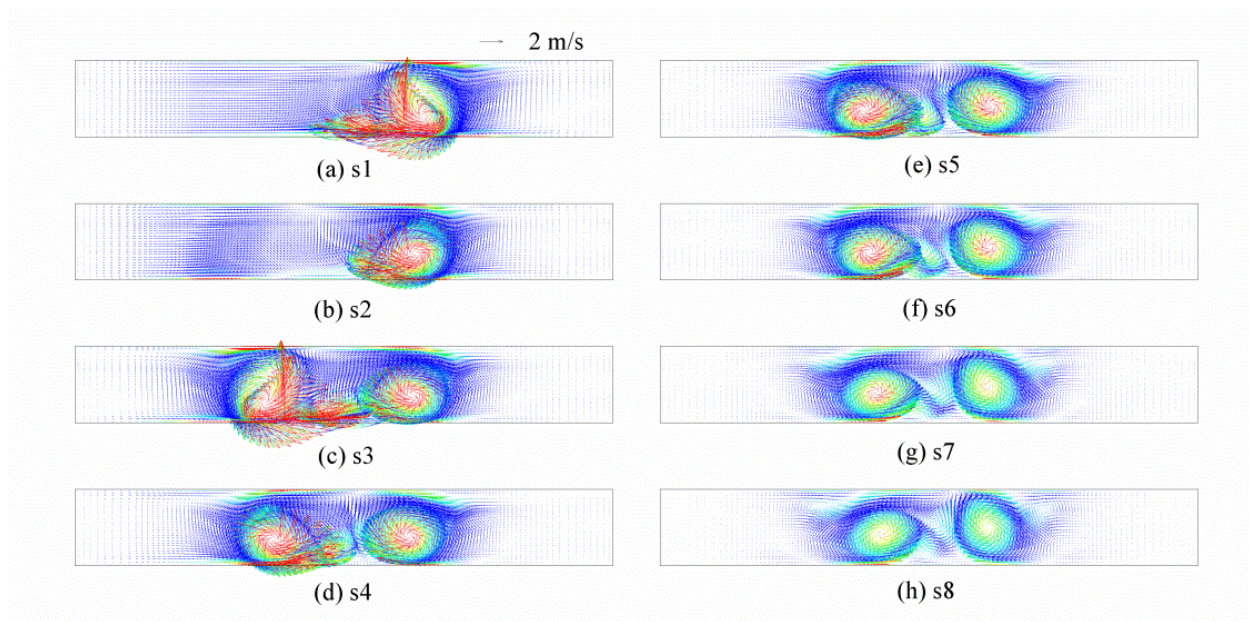


Figure 5. Velocity vectors on the cross sections for transversal pitch $c = c_2$.

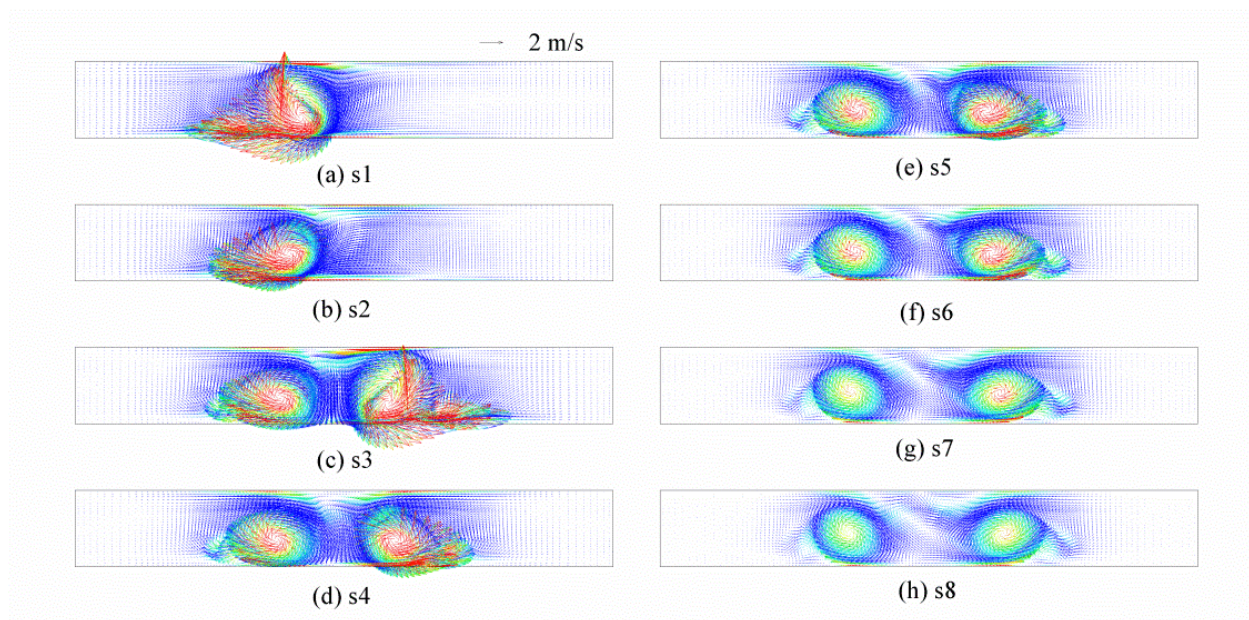


Figure 6. Velocity vectors on the cross sections for transversal pitch $c = c_6$.

The velocity vectors on the cross section s6 with $Re = 1800$ are shown in Figure 7 for different values of c . There are two vortices with counterrotating directions on each cross section. The stronger one with anticlockwise rotating direction is generated by the second VG, and the weaker one with clockwise rotating direction is generated by the first VG. When the value of c changes from c_1 to c_4 , the centers of the vortices move toward the centre of the channel and the distance between the vortices decreases. The interaction between these two counterrotating

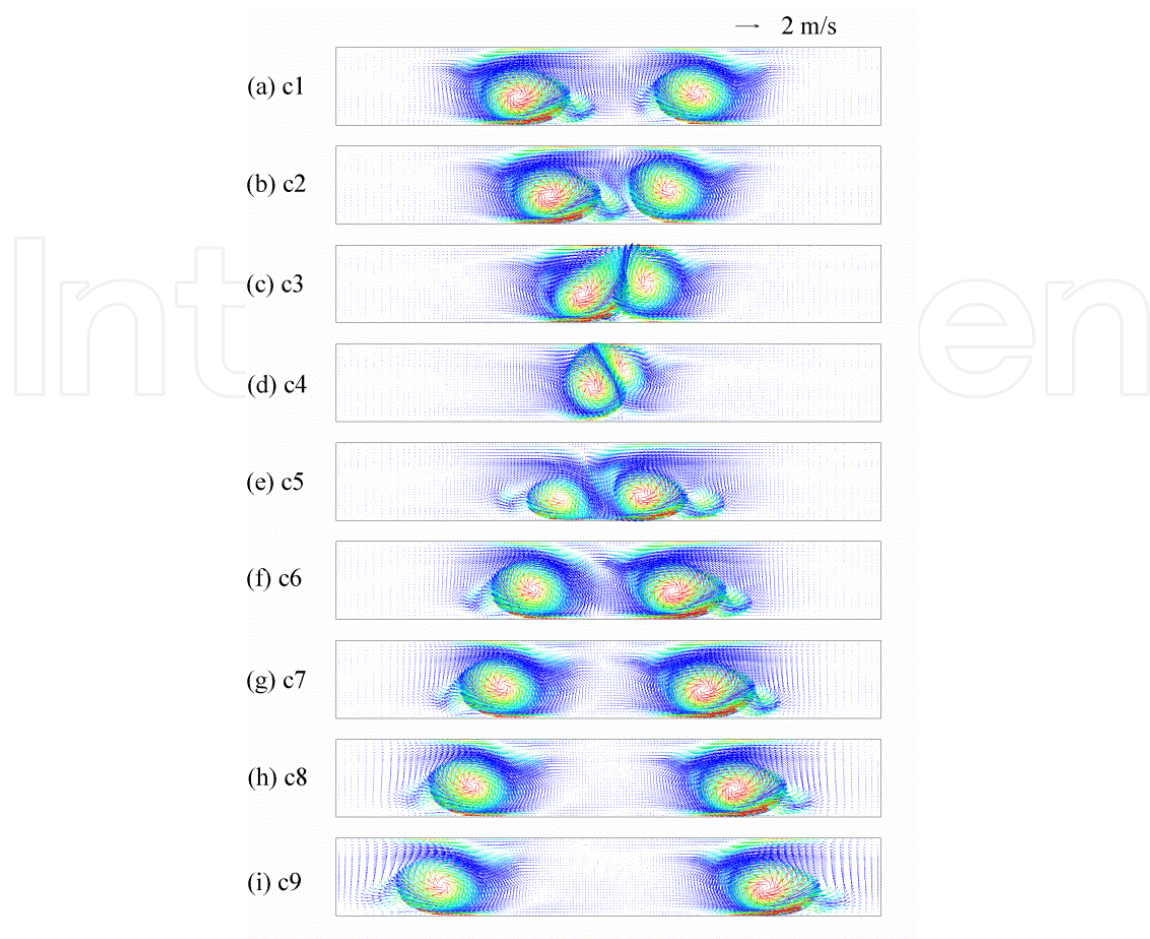


Figure 7. Velocity vectors on the cross sections for different values of c .

vortices increases with decreasing transversal pitch. When the transversal pitch between the VGs is c_4 , the most serious interaction takes place, and the intensity of the vortices becomes weaker. The counterrotating vortices separate from each other when the transversal pitch of VGs changes from c_4 to c_8 . The interaction between the counterrotating vortices decreases, and the intensity of these vortices increases with increasing transversal pitch of VGs. When the counterrotating vortices are located closer to each other, common flow region becomes distinct between the vortices. When the fluid in the common flow region is directed toward the top fin surface, the vortex, especially the weaker one, is directed away from the bottom fin surface. On the contrary, the vortices can be kept at the position close to the bottom fin surface when the fluid in the common flow region is directed toward the bottom fin surface.

6.2. Effect of interaction of longitudinal vortices on Se_s

The parameter Se relates to the intensity of the longitudinal vortices generated by the VGs, and the intensity of these vortices is affected by the interaction between them. Thus, the distribution curve of the span-averaged value of Se along the flow direction can reflect the interaction between the counterrotating longitudinal vortices for different transversal pitches of the VGs.

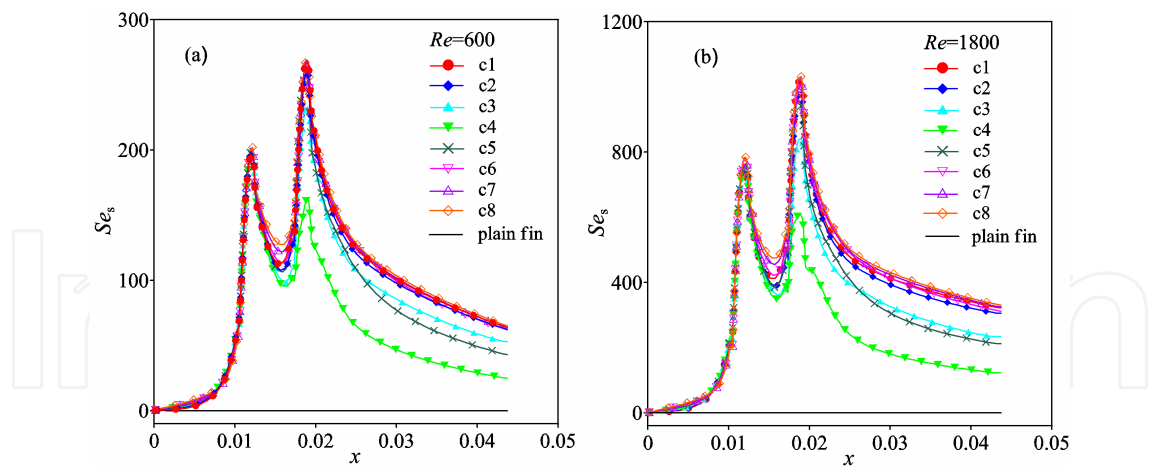


Figure 8. Distribution of Se_s along flow direction.

The distribution of the span-averaged values of Se_s for the range of c are presented in Figure 8 at $Re = 600$ and 1800 . For the flow in the channel formed by plain fin, the fluid flows smoothly and the flow is an irrotational flow; therefore, the vorticity of the irrotational flow is zero. When VGs are added into the fluid, longitudinal vortices are generated by the VGs, and the vorticity of the flow is not zero. The intensity of the vortices changes according to the change of the interaction between the counterrotating longitudinal vortices for different transversal pitches of VGs. In the entrance of the channel, the fluid flows in at a uniform velocity, and the intensity of the vortices is zero. In the region between the entrance and the first VG, the fluid changes flow direction gradually, and the span-averaged value of Se_s also increases gradually from the entrance and then increases rapidly when the fluid passes through the first VG. A peak value of Se_s is obtained at the trailing end of the first VG. Then the value of Se_s decreases rapidly behind the first VG and reaches a peak minimum value in the region between the first and the second VGs. When the fluid passes through the second VG, the value of Se_s increases rapidly and reaches the second peak value at the trailing end of the second VG. Se_s first decreases rapidly just behind the second VG and then becomes smooth till the end of the simulation domain. In the region before the first VG, the distributions of Se_s are nearly the same for all the cases with different transversal pitches. In the region behind the first VG, the distributions of Se_s are different for different values of c due to the interaction between the longitudinal vortices. Evident difference between the distributions of Se_s can be found when the counterrotating longitudinal vortices locate closer to each other. The values of Se_s for the studied cases $c3$, $c4$, and $c5$ are obviously smaller than that for other cases. For the other cases, the interaction between the vortices is weaker, and the differences of Se_s are small. When the transversal pitch of VGs is $c4$, the interaction between the counterrotating longitudinal vortices is the most serious, and the value of Se_s is also the smallest. The peak value of Se_s for $c4$ at the trailing end of the second VG is obviously smaller than the first peak value at the trailing end of the first VG due to the serious interaction between the counterrotating vortices. For the other cases of c , the second peak value of Se_s around the second VG is greater than the first peak value of Se_s around the first VG; the intensity of the vortices increases although interaction also takes place between the counterrotating longitudinal vortices.

6.3. Effect of interaction on Nu_s

Figure 9 shows the distributions of the span-averaged values of Nu_s at $Re = 600$ and 1800 for different values of c . The value of Nu_s for plain fin without VGs is also shown in the figure for comparison. The span-averaged values of Nu_s are obviously enhanced by the longitudinal vortices generated by the VGs mounted in the channel. In the entrance of the channel, the fluid flows in at a uniform velocity, the boundary layer starts to develop, and the value of Nu_s gets the largest value. Then Nu_s decreases rapidly apart from the entrance till the region where the first VG mounted. When the fluid flows around the first VG, Nu_s increases and reaches a peak level at the trailing end of the first VG. Then Nu_s starts to decrease downstream and gets the peak minimum value in the region ahead of the second VG. Nu_s starts to increase in the region where the second VG is mounted and reaches another peak value at the trailing end of the second VG. In the region behind the second VG, owing to the attenuation of vortices, the span-averaged Nu_s decreases rapidly in the beginning and then smoothly till the outlet of the channel. The distributions of Nu_s in the region between the entrance and the second VG are nearly the same for all the cases because the intensity of vortices in this region is not affected by the interaction of counterrotating longitudinal vortices. In the region after the second VG, owing to the interaction between the counterrotating vortices, the differences between the distributions of Nu_s are quite evident, especially for the cases c3, c4, and c5. As the interaction of longitudinal vortices for c4 is the most serious, the decreasing intensity of the vortices weakens the heat transfer performance of the vortices, and the span-averaged Nu_s is the smallest. The peak value of Nu_s at the trailing end of the second VG for c4 is smaller than the peak value at the trailing end of the first VG, but the peak value of Nu_s for c6 is larger than the peak value at the trailing end of the first VG. This means that the interaction between the counterrotating vortices may enhance the heat transfer or decrease the heat transfer.

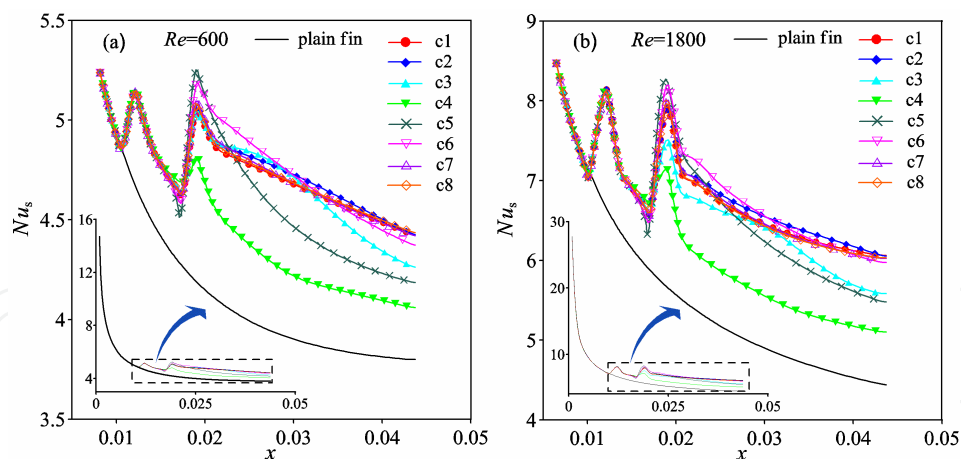


Figure 9. Distribution of Nu_s along flow direction.

The local span-averaged Nu_s for the case c6 is the largest in the region around the second VG. However, the intensity of the longitudinal vortices for the case c6 is not the largest. The reason maybe that a common flow region formed between the VGs and the fluid in the common flow region is directed downwash toward the bottom surface on which the VGs are mounted on, as shown in Figure 6. The heat transfer is locally enhanced benefiting from the local thinning of the thermal boundary layer in the common flow down region. Experimental investigation in reference [4] presents the same conclusion that the heat transfer is locally enhanced in the

region where two neighboring vortices impose a flow toward the surface. Therefore, the interaction of longitudinal vortices does not necessarily decrease the heat transfer performance. The heat transfer performance depends not only on the intensity of the vortices but also on the flow field structure of the vortices.

6.4. Effect of interaction on average values of Se , Nu , and f

The average value of Se over the entire flow and the average value of Nu over the entire area included in the heat transfer are of great interest as they are directly linked to the intensity of longitudinal vortices in the channel and to the amount of total heat transfer. The distributions of Se and Nu for the range of c as a function of Re are presented in Figure 10 (a) and (b), respectively. The values of Se and Nu for the plain fin are also shown for comparison. Both the values of Se and Nu increase monotonically with the increase of Re . The differences between these values also increase with increasing Re , and the differences of Se and Nu for different values of c are quite different. For different values of c , the lowest values of Se and Nu are both obtained for $c = c4$. The values of Se and Nu for $c3$ and $c5$ are nearly the same, and both are larger than that for $c = c5$. For the other cases of c , the values of Se and Nu are larger than that for $c3$, $c4$, and $c5$, but the differences between the values of Se and Nu are very small. Figure 10(c) shows the distributions of friction factor for the range of c studied in this chapter, and the differences between the values of f are quite small. Thus, the interaction between vortices has a very small effect on the friction factor.

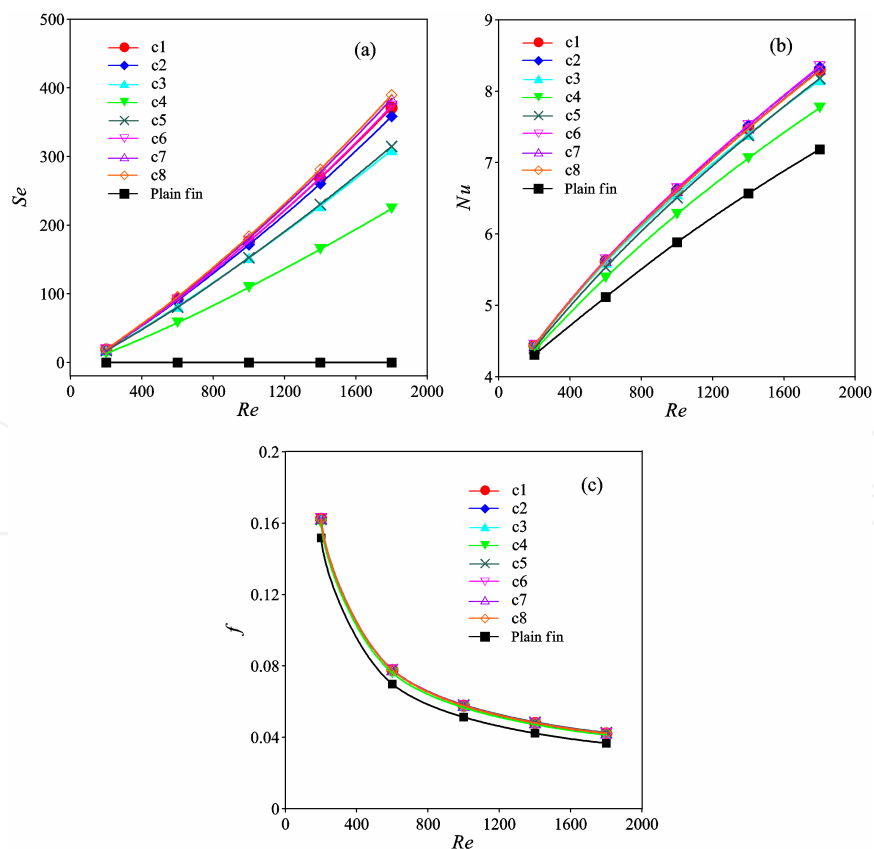


Figure 10. Distribution of Se , Nu , and f for the range of c as a function of Re .

6.5. Effect of interaction on Se/Se_{ref} and Nu/Nu_{ref}

In order to study the effect (in percentage) of the interaction of the counterrotating longitudinal vortices on Se and Nu , the values of Se and Nu for $c1$ are selected as the reference values, then the ratios of Se/Se_{ref} and Nu/Nu_{ref} mean the percentage of Se and Nu compared with the reference values. The distributions of Se/Se_{ref} and Nu/Nu_{ref} as a function of the distance between the VGs are presented in Figure 11 for Re ranging from 200 to 1800. As expected, when values of transversal pitch between the VGs are $c = c3, c4$, and $c5$, the values of Se/Se_{ref} are obviously smaller than those of other configurations, and the ratio of Se/Se_{ref} reaches a peak minimum value at $c = c4$. For other values of c , the differences of Se/Se_{ref} are very small. When the flow in the region between the counterrotating longitudinal vortices is imposed toward the bottom fin surface, the value of Se/Se_{ref} is a little larger than that when a common flow up region between the counterrotating longitudinal vortices is formed.

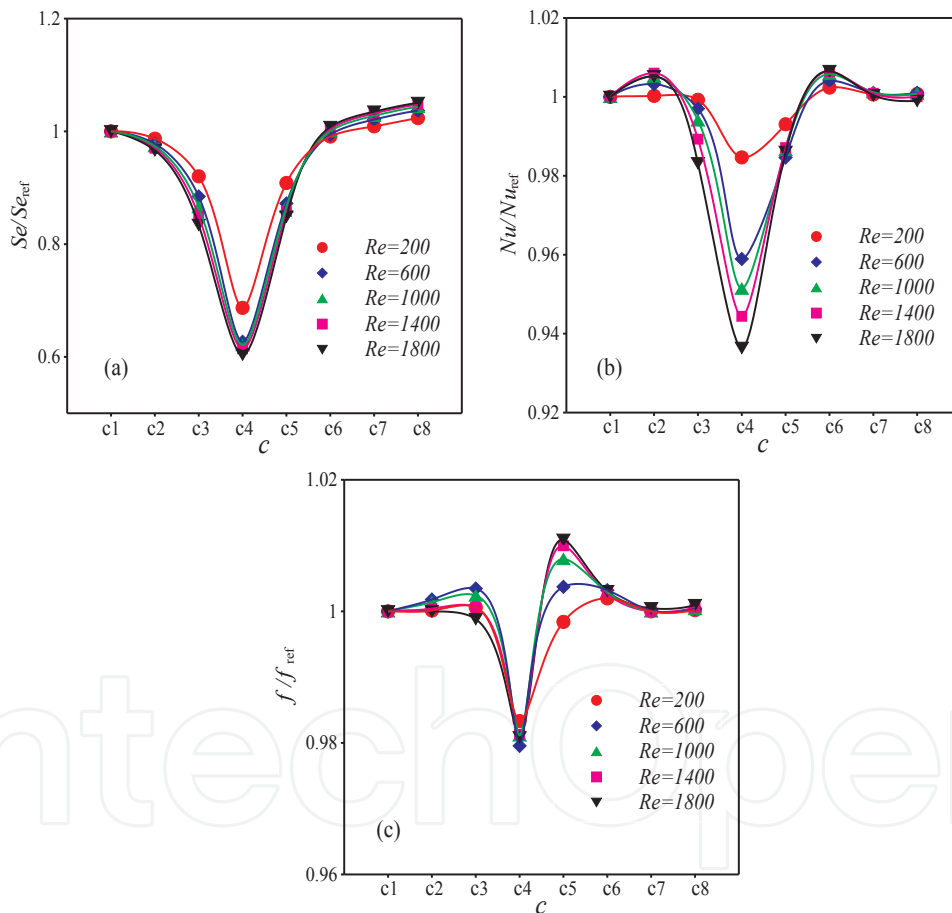


Figure 11. Distributions of Se/Se_{ref} and Nu/Nu_{ref} as a function of c .

The distributions of Nu/Nu_{ref} are much similar to the distributions of Se/Se_{ref} ; the values of Nu/Nu_{ref} also reach the minimum values at $c = c4$. However, the decreasing percentages of Se are not consistent with that of Nu ; the maximum decreasing percentage of Se is about 40%, but it is only about 6% for Nu . The ratio of Nu/Nu_{ref} reaches the peak values at $c = c2$ and $c6$, respectively. This is because when $c = c2$ and $c6$, the interaction between the longitudinal

vortices is relatively small, and the common flow region formed between the VGs is conducive to heat transfer. When $c = c_6$, the fluid in the common flow region is directed downwash toward the bottom fin surface on which the VGs are mounted, and the common flow region imposes fluid toward the top fin surface when $c = c_2$. The fin heat transfer performance is locally enhanced owing to the induced flow in the common flow region. When the distance of c is too large, the common flow region between the vortices will disappear, but when the distance is too small, the intensity of vortices will decrease rapidly due to the interaction between the vortices. Therefore, an optimal arrangement of VGs exists for obtaining a good heat transfer performance of the fin surface mounted with VGs.

6.6. Effect of interaction on JF and JF/JF_{ref}

The surface goodness factor JF under same pump power is more suitable for engineering application and is commonly used as the criteria for evaluating the good performance of heat transfer exchangers or heat transfer surfaces. Figure 12(a) shows the distribution of JF for different values of c as a function of Re. JF increases with increasing Re. When $c = c_3, c_4$, and c_5 , for which there has obvious interaction between the counterrotating longitudinal vortices, the value of JF is obviously smaller than the other cases. When $c = c_4$, the value of JF is the smallest due to the most serious interaction of the counterrotating longitudinal vortices. Figure 12(b) indicates the effect of interaction of longitudinal vortices on the ratio of JF/JF_{ref} for different Re as a function of c . The value of JF for $c = c_1$ is selected as the reference. The distribution of JF/JF_{ref} is similar to the distribution of Nu/Nu_{ref} shown in Figure 11(b). When the transversal pitch between the VGs are $c = c_3, c_4$, and c_5 , the values of JF/JF_{ref} are obviously smaller than the other cases, and the ratio of JF/JF_{ref} decreases with increasing Re. JF/JF_{ref} gets the minimum value at $c = c_4$, and JF is about 5.8% smaller than the reference value at $Re = 1600$. When $c = c_2$ and c_6 , JF/JF_{ref} is greater than 1 and reaches the peak values. Thus, the best heat transfer performance can be obtained at $c = c_2$ and c_6 , for which the distance between the VGs is about twice the projected length of the base length of VGs, that is, $c/(l \sin \theta) = 2.0$.

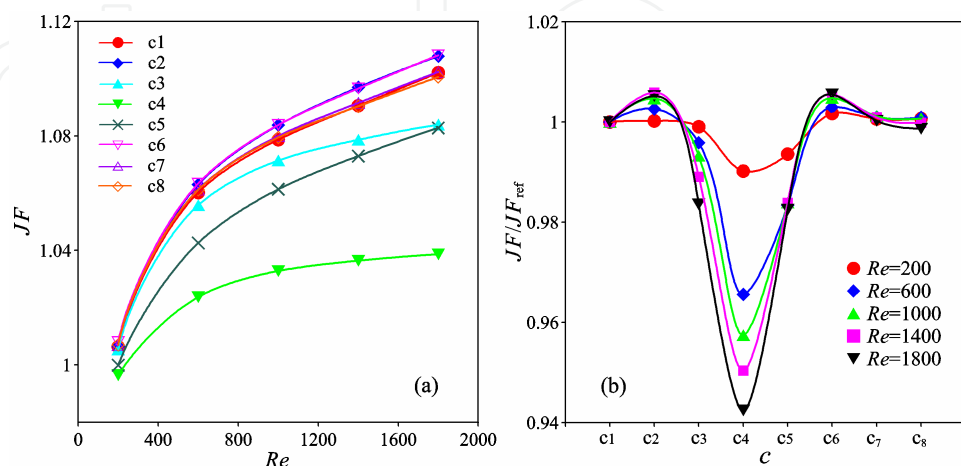


Figure 12. Distributions of JF as a function of Re and JF/JF_{ref} as a function of c .

7. Conclusions

The interaction of two counterrotating longitudinal vortices generated by VGs mounted on the bottom of a channel formed by two neighboring fins and the effect of interaction of counterrotating longitudinal vortices on the intensity of vortices and heat transfer are quantitatively studied using the numerical method. The following conclusions were derived:

- i. The strength of the interaction between the counterrotating vortices is strongly dependent on the transversal pitches between the vortices. The distribution of Se_s does not only reflect the changing of the intensity of the longitudinal vortices in the flow channel but also reflect the interaction between the longitudinal vortices.
- ii. The interaction between the counterrotating longitudinal vortices does not necessarily decrease the intensity of the vortices. When the counterrotating vortices partially interact with each other, the intensity of the vortices can also be increased. When the counterrotating vortices fully interact with each other, the intensity of the vortices decreases seriously.
- iii. The interaction between counterrotating vortices does not necessarily decrease the heat transfer performance of the longitudinal vortices. The heat transfer performance depends on not only the intensity of the vortices but also the structure of the vortices. The common flow region formed between the counterrotating longitudinal vortices is beneficial for the heat transfer enhancement.
- iv. Due to the interactions of counterrotating longitudinal vortices and their effect on heat transfer enhancement, an optimum arrangement of VGs exists for obtaining a better heat transfer performance. When the distance between the VGs is twice the projected length of the base of VGs, the best heat transfer performance can be obtained.

Nomenclature

A ; surface area involved in heat transfer or cross-sectional area (m^2)

$A(x)$; cross-sectional area at position x (m^2)

b ; longitudinal pitch between VGs (m)

c ; transverse pitch between VGs (m)

c_p ; specific heat capacity (J/(kg K))

d_h ; hydraulic diameter, characteristic length (m)

f ; friction factor

h ; height of winglet-type VGs (m) or heat transfer coefficient (W/(m^2 K))

H ; fin spacing (m)

J^n ; vorticity flux in the normal direction of the cross section (1/s)

l ; base length of VG (m)

L ; streamwise length of the simulation domain (m)

n ; direction normal to the cross section

Nu ; Nusselt number: $Nu = hd_h/\lambda$

p ; Pressure loss (Pa)

Re ; Reynolds number: $Re = \rho u_m d_h/\mu$

S ; width of the simulation domain

Se ; secondary flow intensity

T ; temperature (K)

U_s ; characteristic velocity of secondary flow (m/s)

u_m ; maximum average velocity of air (m/s)

u, v, w ; components of velocity vector (m/s)

x, y, z ; coordinates

Greeks

θ ; attack angle of VG ($^\circ$)

λ ; heat conductivity (W/(m K))

μ ; viscosity (kg/(m s))

ρ ; density (kg/m³)

ω ; vorticity (1/s)

Subscripts

ABS; absolute value

bulk; bulk temperature on the cross section

local; local value

s; span-averaged or cross-sectional average value

w; fin surface

Acknowledgements

This work was supported by the National Natural Science Foundation of China (grant nos. 51376086 and 51366008) and the Gansu Provincial Foundation for Distinguished Young Scholars (grant no. 145RJDA324).

Author details

Kewei Song

Address all correspondence to: songkw@mail.lzjtu.cn

School of Mechanical Engineering, Lanzhou Jiaotong University, Lanzhou, Gansu, China

References

- [1] Torri K, Nishino K, Nakayama K. Mechanism of heat transfer augmentation by longitudinal vortices in a flat plate boundary layer. Proceedings of the Tenth International Heat Transfer Conference, Brighton, 1994; 6 123–128.
- [2] Biswas G, Torii K, Fujii D, Nishino K. Numerical and experimental determination of flow structure and heat transfer effects of longitudinal vortices in a channel flow. International Journal of Heat and Mass Transfer 1996; 38 3441–3445.
- [3] Jacobi, AM, Shah RK. Heat transfer surface enhancement through the use of longitudinal vortices: a review of recent progress. Experimental Thermal and Fluid Science 1995; 11 295–309.
- [4] Kataoka K, Doi H, Komai T. Heat mass transfer in Taylor vortex flow with constant axial flow rates. International Journal of Heat and Mass Transfer 1977; 20 57–63.
- [5] Pauley WR And Eaton JK. The effect of embedded longitudinal vortex arrays on turbulent boundary layer heat transfer. Journal of Heat Transfer 1994; 116(4) 871–879.
- [6] Kim WJ, Patel VC. Influence of streamwise curvature on longitudinal vortices embedded in turbulent boundary layers. Computers and Fluids 1994; 23(5) 647–673.
- [7] Zhu ChL, Hua L, Sun DL, Wang LB and Zhang YH. Numerical study of interactions of vortices generated by vortex generators and their effects on heat transfer enhancement. Numerical Heat Transfer, Part A 2006; 50 345–360.
- [8] Song KW, Wang LB. The effectiveness of secondary flow produced by vortex generators mounted on both surfaces of the fin to enhance heat transfer in a flat tube bank fin heat exchanger. ASME Journal of Heat Transfer 2013; 135: 041902.

- [9] Song KW, Wang LB. Interaction of vortices and the augmentation of heat transfer in a flat tube bank fin heat exchanger by vortex generators. The 4th Asian Symposium on Computational Heat Transfer and Fluid Flow, 2013: 91–101, Hong Kong, China.
- [10] Song KW. Numerical research on interaction of longitudinal vortices and the characteristics of fluid flow and heat transfer in the flow channel of exchanger. PhD thesis. Lanzhou Jiaotong University, China; 2014.
- [11] Song, KW, Wang, LB. Relationship between heat transfer intensity and absolute vorticity flux intensity in flat tube bank fin channels with vortex generators. Progress in Computational Fluid Dynamics 2008; 8 (7–8) 496–502.
- [12] Chang LM, Wang LB, Song KW. Numerical study of the relationship between heat transfer enhancement and absolute vorticity flux along main flow direction in a channel formed by a flat tube bank fin with vortex generators. International Journal of Heat and Mass Transfer 2009; 52 1794–1801.

